Journal of Computational and Applied Mathematics 235 (2010) 229–243

Contents lists available at ScienceDirect

Journal of Computational and Applied Mathematics

journal homepage: www.elsevier.com/locate/cam

A self-adaptive moving mesh method for the Camassa–Holm equation

Bao-Feng Feng [a,*], Ken-ichi Maruno [a], Yasuhiro Ohta [b]

[a] Department of Mathematics, The University of Texas-Pan American, Edinburg, TX 78539-2999, USA

[b] Department of Mathematics, Kobe University, Rokko, Kobe 657-8501, Japan

ARTICLE INFO

Article history:
Received 15 December 2009
Received in revised form 27 April 2010

MSC:
65M06
35Q58
37K40

Keywords:
The Camassa–Holm equation
Integrable semi-discretization
Peakon and cupson solutions
Self-adaptive moving mesh method

ABSTRACT

A self-adaptive moving mesh method is proposed for the numerical simulations of the Camassa–Holm equation. It is an integrable scheme in the sense that it possesses the exact N-soliton solution. It is named a self-adaptive moving mesh method, because the non-uniform mesh is driven and adapted automatically by the solution. Once the non-uniform mesh is evolved, the solution is determined by solving a tridiagonal linear system. Due to these two superior features of the method, several test problems give very satisfactory results even if by using a small number of grid points.

1. Introduction

Since its discovery [1], the Camassa–Holm (CH) equation

$$w_T + 2\kappa w_X - w_{TXX} + 3ww_X = 2w_X w_{XX} + ww_{XXX} \tag{1}$$

has attracted considerable interest because it describes unidirectional propagation of shallow water waves on a flat bottom. It also appeared in a mathematical search of recursion operators connected with the integrable partial differential equations [2]. By virtue of asymptotic procedures, the CH equation was reconfirmed as a valid approximation to the governing equation for shallow water waves [3,4]. The CH equation also arises as a model for water waves moving over an underlying shear flow [5], in the study of a certain non-Newtonian fluids [6], and as a model for nonlinear waves in cylindrical hyperelastic rods [7]. The CH equation is completely integrable (see [1] for the Lax pair formulation and [8,9] for the inverse scattering transform), and it has various exact solutions such as solitons, peakons, and cuspons. When $\kappa = 0$, the CH equation admits peakon solutions which are represented by piecewise functions [1,10,11]. When $\kappa \neq 0$, cusped soliton (cuspon) solutions, as well as smooth soliton solutions, were found by several authors. [12–19].

Several numerical schemes have been proposed for the CH equation in the literature. These include a pseudospectral method [20], finite difference schemes [21,22], a finite volume method [23], finite element methods [24–26], multi-symplectic methods [27], and a particle method in terms of characteristics based on the multi-peakon solution [28–32]. We comment that the schemes in [21,22] and in [27] can handle peakon–antipeakon interactions. However, it still remains a challenging problem for the numerical integration of the CH equation due to the singularities of cuspon and peakon solutions.

In the present paper, we will study an integrable difference scheme for the CH equation (1) based on an integrable semi-discrete CH equation proposed by the authors [33]. The scheme consists of an algebraic equation for the solution and the

* Corresponding author.
E-mail address: feng@utpa.edu (B.-F. Feng).

0377-0427/$ – see front matter © 2010 Published by Elsevier B.V.
doi:10.1016/j.cam.2010.05.044

non-uniform mesh for a fixed time, and a time evolution equation for the mesh. Since the mesh is automatically driven and adapted by the solution, we name it a self-adaptive moving mesh method hereafter.

As a matter of fact, Harten and Hyman have proposed a self-adjusting grid method for one-dimensional hyperbolic problems [34]. Since then, there has been significant progress in developing adaptive mesh methods for PDEs [35–40]. These methods have been successfully applied to a variety of physical and engineering problems with singular or nearly singular solutions developed in fairly localized regions, such as shock waves, boundary layers, detonation waves, etc. Recently, an adaptive unwinding method was proposed for the CH equation [23]. The method is high resolution and stable. However, in order to achieve a good accuracy, a large number of grid points (=4096) has to be used. In addition, the designed method is only suitable for the single peakon propagation and peakon–peakon interactions, not for the peakon–antipeakon interaction. As shown subsequently, the self-adaptive moving mesh method gives accurate results by using a small number of grid points ($\approx$100) for some challenging test problems.

The remainder of this paper is organized as follows. In Section 2, we present the self-adaptive moving mesh method and show it is consistent with the CH equation as the mesh size approaches to zero. Two time advancing methods in implementing the self-adaptive moving mesh method are presented in Section 3. In Section 4, several numerical experiments, including the propagations of "peakon" and "cuspon" solutions, cuspon–cuspon and soliton–cuspon collisions, are shown. The concluding remarks are addressed in Section 5.

2. A self-adaptive moving mesh method for the Camassa–Holm equation

It is shown in [33] that the CH equation can be derived from the bilinear equations of a deformation of the modified KP hierarchy

$$\begin{cases} -\left(\frac{1}{2}D_tD_x - 1\right) f\cdot f = gh, \\ 2cff = (D_x + 2c)g\cdot h, \\ -2ff = (D_tD_x + 2cD_t - 2)g\cdot h, \end{cases} \tag{2}$$

through the hodograph transformation

$$\begin{cases} X = 2cx + \log\frac{g}{h}, \\ T = t, \end{cases} \tag{3}$$

and the dependent variable transformation

$$w = \left(\log\frac{g}{h}\right)_t.$$

Here $c = 1/\kappa$, D_x and D_t are Hirota's D-operator defined as

$$D_x^n f\cdot g = \left(\frac{\partial}{\partial x} - \frac{\partial}{\partial y}\right)^n f(x)g(y)\Big|_{y=x}.$$

It is proved in [33] that the bilinear equations (2) admit a determinant solution $f = \tau_0, g = \tau_{-1}, h = \tau_1$, where τ_n is a Casorati-type determinant of any size. By discretizing the x-direction with an uniform mesh size a, the following bilinear equations

$$\begin{cases} -2\left(\frac{1}{a}D_t - 1\right) f_{k+1}\cdot f_k = g_{k+1}h_k + g_kh_{k+1}, \\ 2acf_{k+1}f_k = (1+ac)g_{k+1}h_k - (1-ac)g_kh_{k+1}, \\ -2af_{k+1}f_k = ((1+ac)D_t - a)g_{k+1}\cdot h_k - ((1-ac)D_t + a)g_k\cdot h_{k+1}, \end{cases} \tag{4}$$

admit a Casorati-type determinant solution with a discrete index which is presented afterwards. Starting from Eq. (4), a semi-discrete CH equation

$$\begin{cases} -2\left(\frac{w_{k+1}-w_k}{\delta_k} - \frac{w_k - w_{k-1}}{\delta_{k-1}}\right) + \delta_k\frac{w_{k+1}+w_k}{2} + \frac{\delta_k}{c}\frac{1-\frac{4a^2c^2}{\delta_k^2}}{1-a^2c^2} + \delta_{k-1}\frac{w_k+w_{k-1}}{2} + \frac{\delta_{k-1}}{c}\frac{1-\frac{4a^2c^2}{\delta_{k-1}^2}}{1-a^2c^2} = 0, \\ \frac{\mathrm{d}\,\delta_k}{\mathrm{d}t} = \left(1 - \frac{\delta_k^2}{4}\right)(w_{k+1} - w_k) \end{cases} \tag{5}$$

was proposed (see the details in [33]). Here the solution $w(X_k, t)$ is approximated by $w_k(t)$ at the grid points X_k ($k = 1, \ldots, N$). The mesh $\delta_k = X_{k+1} - X_k$ is a discrete analogue of the hodograph transformation from the x-domain with uniform mesh size a to X-domain. As is seen, it is non-uniform and time-dependent.

The semi-discrete CH equation (5) can be rewritten as

$$\begin{cases} \Delta^2 w_k = \dfrac{1}{\delta_k} M\left(\delta_k M w_k + \dfrac{1}{c\delta_k}\dfrac{\delta_k^2/c^2 - 4a^2}{1/c^2 - a^2}\right), \\ \dfrac{\mathrm{d}\delta_k}{\mathrm{d}t} = \left(1 - \dfrac{\delta_k^2}{4}\right)\delta_k \Delta w_k \end{cases} \tag{6}$$

by introducing a forward difference operator and an average operator Δ and M

$$\Delta F_k = \frac{F_{k+1} - F_k}{\delta_k}, \qquad MF_k = \frac{F_k + F_{k+1}}{2}.$$

In the present paper, Eq. (5) or Eq. (6) is used as a numerical scheme for the CH equation (1). It is shown to be integrable in [33] in the sense that it possesses an N-soliton solution which, in the continuous limit, approaches an N-soliton solution of the CH equation. The N-soliton solution is of the form

$$w_k = \left(\log \frac{g_k}{h_k}\right)_t, \tag{7}$$

with

$$f_k = \tau_0(k), \qquad g_k = \tau_1(k), \qquad h_k = \tau_{-1}(k),$$
$$\tau_n(k) = \begin{vmatrix} \psi_1^{(n)} & \psi_1^{(n+1)} & \cdots & \psi_1^{(n+N-1)} \\ \psi_2^{(n)} & \psi_2^{(n+1)} & \cdots & \psi_2^{(n+N-1)} \\ \vdots & \vdots & & \vdots \\ \psi_N^{(n)} & \psi_N^{(n+1)} & \cdots & \psi_N^{(n+N-1)} \end{vmatrix}$$

where

$$\psi_i^{(n)} = a_{i,1}(p_i - c)^n(1 - ap_i)^{-k}\mathrm{e}^{\xi_i} + a_{i,2}(-p_i - c)^n(1 + ap_i)^{-k}\mathrm{e}^{\eta_i},$$
$$\xi_i = \frac{1}{p_i - c}t + \xi_{i0}, \qquad \eta_i = -\frac{1}{p_i + c}t + \eta_{i0}.$$

Next, let us show that in the continuous limit, $a \to 0$ ($\delta_k \to 0$), the proposed scheme is consistent with the CH equation. To this end, the Eq. (6) is rewritten as

$$\begin{cases} \dfrac{-2}{\delta_k + \delta_{k-1}}(\Delta w_k - \Delta w_{k-1}) + \dfrac{\delta_k M w_k}{\delta_k + \delta_{k-1}} + \dfrac{\delta_{k-1} M w_{k-1}}{\delta_k + \delta_{k-1}} + \dfrac{1}{c(1 - a^2c^2)} = \dfrac{4a^2c}{1 - a^2c^2}\dfrac{1}{\delta_k\delta_{k-1}}, \\ \partial_t \delta_k = \left(1 - \dfrac{\delta_k^2}{4}\right)(w_{k+1} - w_k). \end{cases}$$

By taking the logarithmic derivative of the first equation, we get

$$\begin{cases} \dfrac{\partial_t\left\{\frac{2}{\delta_k+\delta_{k-1}}(\Delta w_k - \Delta w_{k-1}) - \frac{\delta_k M w_k}{\delta_k+\delta_{k-1}} - \frac{\delta_{k-1} M w_{k-1}}{\delta_k+\delta_{k-1}}\right\}}{\frac{2}{\delta_k+\delta_{k-1}}(\Delta w_k - \Delta w_{k-1}) - \frac{\delta_k M w_k}{\delta_k+\delta_{k-1}} - \frac{\delta_{k-1} M w_{k-1}}{\delta_k+\delta_{k-1}} - \frac{1}{c(1-a^2c^2)}} = -\dfrac{\partial_t\delta_k}{\delta_k} - \dfrac{\partial_t\delta_{k-1}}{\delta_{k-1}}, \\ \partial_t \delta_k = \left(1 - \dfrac{\delta_k^2}{4}\right)(w_{k+1} - w_k). \end{cases}$$

Thus, we have

$$\frac{\partial_t\left\{\frac{2}{\delta_k+\delta_{k-1}}(\Delta w_k - \Delta w_{k-1}) - \frac{\delta_k M w_k}{\delta_k+\delta_{k-1}} - \frac{\delta_{k-1} M w_{k-1}}{\delta_k+\delta_{k-1}}\right\}}{\frac{2}{\delta_k+\delta_{k-1}}(\Delta w_k - \Delta w_{k-1}) - \frac{\delta_k M w_k}{\delta_k+\delta_{k-1}} - \frac{\delta_{k-1} M w_{k-1}}{\delta_k+\delta_{k-1}} - \frac{1}{c(1-a^2c^2)}} = -\left(1 - \frac{\delta_k^2}{4}\right)\Delta w_k - \left(1 - \frac{\delta_{k-1}^2}{4}\right)\Delta w_{k-1}.$$

The dependent variable w is a function of k and t, and we regard them as a function of X and T, where X is the space coordinate of the k-th lattice point and T is the time, defined by

$$X = X_0 + \sum_{j=0}^{k-1}\delta_j, \qquad T = t.$$

Then in the continuous limit, $a \to 0$ ($\delta_k \to 0$), we have

$$\Delta w_k \to w_X, \qquad \Delta w_{k-1} \to w_X, \qquad M w_k \to w, \qquad \Delta w_{k-1} \to w_X,$$

and

$$\frac{2}{\delta_k+\delta_{k-1}}(\Delta w_k-\Delta w_{k-1})\to w_{XX}.$$

Further, from

$$\frac{\partial X}{\partial t}=\frac{\partial X_0}{\partial t}+\sum_{j=0}^{k-1}\frac{\partial \delta_j}{\partial t}=\frac{\partial X_0}{\partial t}+\sum_{j=0}^{k-1}\left(1-\frac{\delta_j^2}{4}\right)(w_{j+1}-w_j)\to w,$$

we have

$$\partial_t=\partial_T+\frac{\partial X}{\partial t}\partial_X\to\partial_T+w\partial_X,$$

where the origin of space coordinate X_0 is taken so that $\frac{\partial X_0}{\partial t}$ cancels w_0. Then the above semi-discrete CH equation converges to the CH equation

$$\frac{(\partial_T+w\partial_X)(w_{XX}-w)}{w_{XX}-w-\frac{1}{c}}=-2w_X,$$

i.e.

$$(\partial_T+w\partial_X)(w_{XX}-w)=-2w_X\left(w_{XX}-w-\frac{1}{c}\right). \tag{8}$$

Setting $c=1/\kappa$, we obtain the CH equation (1).

Note that, in our previous paper [33], we put $c=1/\kappa^2$ which gives an alternative form of the CH equation

$$w_T+2\kappa^2w_X-w_{TXX}+3ww_X=2w_Xw_{XX}+ww_{XXX}. \tag{9}$$

It is shown that they are equivalent under the scaling transformation $w\to\kappa w, T\to T/\kappa$. In the present paper, for the convenience in comparing our results with other papers [14–19,41], we set $c=1/\kappa$.

3. Implementation of the self-adaptive moving mesh method

In this section, we will discuss how to implement the self-adaptive moving mesh method in actual computations. Generally, given an arbitrary initial condition $w(X,0)=w_0(X)$, the initial non-uniform mesh δ_k can be obtained by solving the nonlinear algebraic equations by Newton's iteration method. However, for the propagation or interaction of solitons or cuspons, which are challenging problems numerically, the initial condition w_k can be calculated by (7) from g_k and h_k by putting $t=0$, which are obtainable from the corresponding determinant solutions. The initial non-uniform mesh δ_k^0 can also be calculated by [33]

$$\delta_k^0=2\frac{(1+ac)g_{k+1}h_k-(1-ac)g_kh_{k+1}}{(1+ac)g_{k+1}h_k+(1-ac)g_kh_{k+1}}. \tag{10}$$

On the other hand, once the non-uniform mesh δ_k is known, the solution w_k can be easily obtained by solving a tridiagonal linear system based on the first equation of the scheme.

$$a_lw_{l-1}^{n+1}+b_lw_l^{n+1}+c_lw_{l+1}^{n+1}=d_l, \tag{11}$$

where

$$a_l=0.5\delta_{k-1}^{n+1}-\frac{2}{\delta_{k-1}^{n+1}};\qquad b_l=0.5(\delta_{k-1}^{n+1}+\delta_k^{n+1})+\frac{2}{\delta_{k-1}^{n+1}}+\frac{2}{\delta_k^{n+1}};\qquad c_l=0.5\delta_k^{n+1}-\frac{2}{\delta_k^{n+1}};$$

and

$$d_l=\frac{4a^2c}{1-a^2c^2}\left(\frac{1}{\delta_k^{n+1}}+\frac{1}{\delta_{k-1}^{n+1}}\right)-\frac{\delta_{k-1}^{n+1}+\delta_k^{n+1}}{c(1-a^2c^2)}.$$

In regard to the evolution of δ_k, we propose two time advancing methods. The first is the modified forward Euler method, where we assume w_k remains unchanged in one time step. Integrating once, we have

$$\delta_k^{n+1}=2\frac{c_k^ne^{(w_{k+1}^n-w_k^n)\Delta t}-1}{c_k^ne^{(w_{k+1}^n-w_k^n)\Delta t}+1}, \tag{12}$$

where $c_k^n = (2+\delta_k^n)/(2-\delta_k^n)$. The second is the classical 4th-order Runge–Kutta method, where w_k can be viewed as a function of δ_k by solving the above tridiagonal linear system. Therefore, in one time step, we have to solve tridiagonal linear system four times.

In summary, the numerical computation in one time-step only involves an ODE solver for a non-uniform mesh and a tridiagonal linear system solver. Hence, the computation cost is much less than other existing numerical methods. A Matlab code is made to perform all the computations. Iterative methods, for instance, the bi-conjugate gradient method bicg in Matlab are used to solve the tridiagonal system.

For the sake of numerical experiments in the subsequent section, we list exact one- and two- soliton/cuspon and peakon solutions.

(1). *One soliton/cuspon solution*: The τ-functions for the one soliton/cuspon solution are

$$g \propto 1 \pm \left(\frac{c-p_1}{c+p_1}\right) \mathrm{e}^{\xi_1}, \qquad h \propto 1 \pm \left(\frac{c+p_1}{c-p_1}\right) \mathrm{e}^{\xi_1}, \tag{13}$$

with $\xi_1 = p_1(2x - v_1 t - x_{10})$, $v_1 = 2/(c^2 - p_1^2)$. This leads to a solution

$$w(x,t) = \frac{2p_1^2 c v_1}{(c^2+p_1^2) \pm (c^2-p_1^2)\cosh\xi_1}, \tag{14}$$

$$X = 2cx + \log\left(\frac{g}{h}\right), \qquad T = t, \tag{15}$$

where the positive case in Eq. (14) stands for the one smooth soliton solution when $p_1 < c$, while the negative case in Eq. (14) stands for the one-cuspon solution when $p_1 > c$. Otherwise, the solution is singular. Thus Eq. (14) for nonsingular cases can be expressed by

$$w(x,t) = \frac{2p_1^2 c v_1}{(c^2+p_1^2) + |c^2-p_1^2|\cosh\xi_1}. \tag{16}$$

Similarly, for the semi-discrete case, we have

$$g_k \propto 1 + \left|\frac{c-p_1}{c+p_1}\right| \left(\frac{1+ap_1}{1-ap_1}\right)^k \mathrm{e}^{\xi_1}, \qquad h_k \propto 1 + \left|\frac{c+p_1}{c-p_1}\right| \left(\frac{1+ap_1}{1-ap_1}\right)^k \mathrm{e}^{\xi_1}, \tag{17}$$

with $\xi_1 = p_1(-v_1 t - x_{10})$, resulting in a solution of the form

$$w_k(t) = \frac{2p_1^2 c v_1}{(c^2+p_1^2) + \frac{|c^2-p_1^2|}{2}\left[\left(\frac{1+ap_1}{1-ap_1}\right)^{-k} \mathrm{e}^{-\xi_1} + \left(\frac{1+ap_1}{1-ap_1}\right)^{k} \mathrm{e}^{\xi_1}\right]}, \tag{18}$$

in conjunction with a transform between an uniform mesh a and a non-uniform mesh

$$\delta_k = 2\frac{(1+ac)g_{k+1}h_k - (1-ac)g_k h_{k+1}}{(1+ac)g_{k+1}h_k + (1-ac)g_k h_{k+1}}.$$

(2). *Two soliton/cuspon solutions*: The τ-functions for the two soliton/cuspon solution are

$$g \propto 1 + \left|\frac{c-p_1}{c+p_1}\right| \mathrm{e}^{\xi_1} + \left|\frac{c-p_2}{c+p_2}\right| \mathrm{e}^{\xi_2} + \left|\frac{(c-p_1)(c-p_2)}{(c+p_1)(c+p_2)}\right| \left(\frac{p_1-p_2}{p_1+p_2}\right)^2 \mathrm{e}^{\xi_1+\xi_2},$$

$$h \propto 1 + \left|\frac{c+p_1}{c-p_1}\right| \mathrm{e}^{\xi_1} + \left|\frac{c+p_2}{c-p_2}\right| \mathrm{e}^{\xi_2} + \left|\frac{(c+p_1)(c+p_2)}{(c-p_1)(c-p_2)}\right| \left(\frac{p_1-p_2}{p_1+p_2}\right)^2 \mathrm{e}^{\xi_1+\xi_2},$$

with $\xi_1 = p_1(2x - v_1 t - x_{10})$, $\xi_2 = p_2(2x - v_2 t - x_{20})$, $v_1 = 2/(c^2 - p_1^2)$, $v_2 = 2/(c^2 - p_2^2)$. The parametric solution can be calculated through

$$w(x,t) = \left(\log\frac{g}{h}\right)_t, \qquad X = 2cx + \log\left(\frac{g}{h}\right), \qquad T = t, \tag{19}$$

whose form is complicated and is omitted here. Note that the above expression includes the two-soliton solution ($p_1 < c, p_2 < c$), the two-cuspon solution ($p_1 > c, p_2 > c$), or the soliton–cuspon solution ($p_1 < c, p_2 > c$).

Similarly, for the semi-discrete case, we have

$$g_k \propto 1 + \left|\frac{c-p_1}{c+p_1}\right| \left(\frac{1+ap_1}{1-ap_1}\right)^k \mathrm{e}^{\xi_1} + \left|\frac{c-p_2}{c+p_2}\right| \left(\frac{1+ap_2}{1-ap_2}\right)^k \mathrm{e}^{\xi_2} + \left|\frac{(c-p_1)(c-p_2)}{(c+p_1)(c+p_2)}\right| \left(\frac{p_1-p_2}{p_1+p_2}\right)^2 \left(\frac{1+ap_1}{1-ap_1}\right)^k \left(\frac{1+ap_2}{1-ap_2}\right)^k \mathrm{e}^{\xi_1+\xi_2},$$

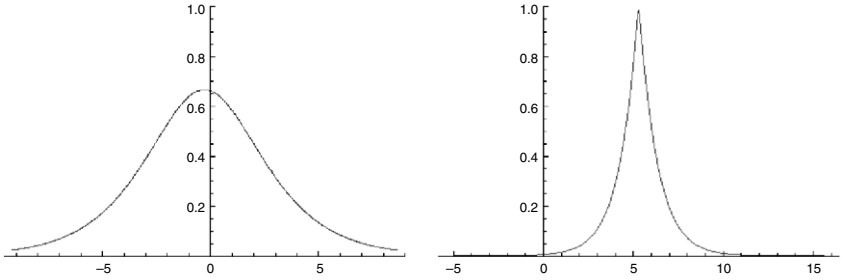

Fig. 1. 1-soliton solution for the CH equation: the left: $p_1 = 0.5$, $c = 1$; the right (close to the peakon limit): $p_1 = 99$, $c = 100$.

$$h_k \propto 1 + \left|\frac{c+p_1}{c-p_1}\right| \left(\frac{1+ap_1}{1-ap_1}\right)^k e^{\xi_1} + \left|\frac{c+p_2}{c-p_2}\right| \left(\frac{1+ap_2}{1-ap_2}\right)^k e^{\xi_2} + \left|\frac{(c+p_1)(c+p_2)}{(c-p_1)(c-p_2)}\right| \left(\frac{p_1-p_2}{p_1+p_2}\right)^2 \left(\frac{1+ap_1}{1-ap_1}\right)^k \left(\frac{1+ap_2}{1-ap_2}\right)^k e^{\xi_1+\xi_2},$$

with $\xi_1 = p_1(-v_1 t - x_{10})$, $\xi_2 = p_2(-v_2 t - x_{20})$. The solution can be calculated through

$$w(x,t) = \left(\log \frac{g_k}{h_k}\right)_t, \tag{20}$$

with a transform

$$\delta_k = 2\frac{(1+ac)g_{k+1}h_k - (1-ac)g_k h_{k+1}}{(1+ac)g_{k+1}h_k + (1-ac)g_k h_{k+1}}. \tag{21}$$

Again, the explicit form of the solution is complicated and is omitted here.

(3). *Peakon solutions*: In the continuous CH equation, it is possible to construct peakon solutions from soliton solutions by taking the peakon limit [10,42,12,14,16,43,41].

For the continuous case, we can express the 1-soliton solution as

$$w = \frac{2p_1^2\kappa v_1}{1 + p_1^2\kappa^2 + (1 - p_1^2\kappa^2)\cosh\xi_1},$$

where $\kappa = \frac{1}{c}$, $v_1 = 2\kappa^2/(1 - p_1^2\kappa^2)$, $\xi_1 = p_1\kappa(2x/\kappa - (v_1/\kappa)t - x_{10}/\kappa)$. Taking the peakon limit $\kappa \to 0$, $p_1\kappa \to 1$, $v_1 =$ const., the solution $(X(x,t), w(x,t))$, where $X(x,t) = 2x/\kappa + \log\frac{g}{h}$, gives the 1-peakon solution [41]. In Fig. 1, one can see that the 1-soliton solution approaches the 1-peakon solution as κ approaches to 0.

We can also consider the peakon limit for the semi-discrete CH equation. For the semi-discrete case, we can express the 1-soliton solution as

$$w_k = \frac{2p_1^2\kappa v_1}{1 + p_1^2\kappa^2 + \frac{1-p_1^2\kappa^2}{2}\left[\left(\frac{1+ap_1}{1-ap_1}\right)^{-k} e^{-\xi_1} + \left(\frac{1+ap_1}{1-ap_1}\right)^k e^{\xi_1}\right]},$$

where $\kappa = \frac{1}{c}$, $v_1 = 2\kappa^2/(1 - p_1^2\kappa^2)$, $\xi_1 = p_1\kappa(-(v_1/\kappa)t - x_{10}/\kappa)$. The peakon limit for the semi-discrete CH equation is again $\kappa \to 0$, $p_1\kappa \to 1$, $v_1 =$ const. Taking the peakon limit, the solution $(X_k(t), w_k(t))$, where $X_k(t) = X_0 + \sum_{j=0}^{k-1}\delta_j(t)$, approaches a solution which approaches the peakon solution of the CH equation as taking the continuous limit. In Fig. 2, one can see that the 1-soliton solution approaches the 1-peakon like solution as κ approaches 0. Taking the continuous limit, this solution approaches the 1-peakon solution of the CH equation.

4. Numerical experiments

In this section, we apply our scheme to several test problems. They include: (1) propagation and interaction of nearly-peakon solutions; (2) propagation and interaction of cuspon solutions; (3) interactions of soliton–cuspon solutions; (4) non-exact initial value problems.

4.1. Propagation and interaction of nearly-peakon solutions

Example 1 (*One Peakon Propagation*)**.** It has been shown in [43,41] that the analytic N-soliton solution of the CH equation converges to the nonanalytic N-peakon solution when $\kappa \to 0$ ($c \to \infty$). To show this, we choose one soliton solution with

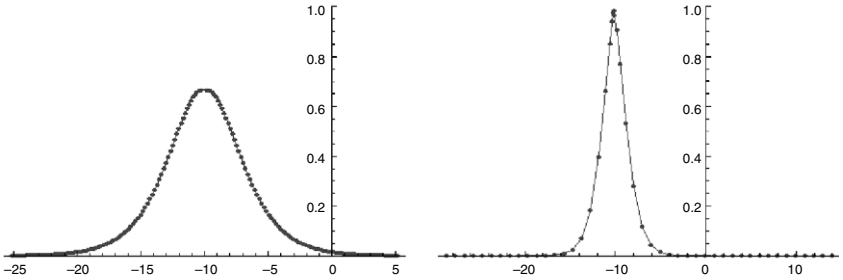

Fig. 2. 1-soliton solution for the semi-discrete CH equation: the left: $p_1 = 0.5$, $c = 1$, $a = 0.1$; the right (close to the peakon limit): $p_1 = 99$, $c = 100$, $a = 0.005$.

Table 1
Comparison of L_∞ and I_1 errors for one-soliton propagation.

	Δt	T	L_∞	E_1
MFE	0.001	2.0	6.9(−4)	8.1(−4)
	0.001	4.0	1.4(−3)	1.6(−3)
RK4	0.01	2.0	1.7(−12)	4.5(−13)
	0.01	4.0	5.4(−12)	8.4(−13)

Table 2
L_∞ and I_1 errors for two approximate peakon interaction by the self-adaptive moving mesh method.

	Δt	T	L_∞	E_1
MFE	0.001	5.0	2.2(−2)	5.5(−3)
	0.001	10.0	7.1(−2)	1.2(−2)
RK4	0.01	5.0	2.0(−9)	1.5(−7)
	0.01	10.0	3.2(−9)	1.4(−5)

parameters $c = 1000$, $p = 998.9995$. Thus the speed of the soliton ($v_1/2$) is 1.0. Its profile is plotted and is compared with one peakon solution $u(x, t) = e^{-|x-t|}$ in Fig. 3. These two solutions are indistinguishable from the graph. The error in L_∞, where $L_\infty = \max |w_l - u_l|$, is calculated to be $O(10^{-3})$, and the discrepancy for the first conserved quantity $I_1 = \int u\,dx$ is less than 0.7%. Therefore, this soliton solution can be viewed as an approximate peakon solution with amplitude 1.0.

The propagation of the above designed approximate peakon solution is solved by the self-adaptive mesh scheme with two different time advancing methods: the modified forward Euler method (MFE) and the classical Runge–Kutta method (RK4). The length of the interval in the x-domain is chosen to be 0.02 and the number of grid points is $N = 101$. For the above parameters of one-peakon solution, the length of the computation domain turns out to be about 28.5. Fig. 4 (a)–(d) display the numerical solutions at $t = 1.0, 2.0, 3.0, 4.0$, together with the self-adjusted mesh. It can be seen that the non-uniform mesh is dense around the crest. The most dense part of the non-uniform mesh moves along with the peakon point with the same speed. With the same grid points $N = 101$, the relative errors in L_∞-norm and the first conserved quantity $I_1 = \int w\,dx$ are computed and compared in Table 1. Here, $L_\infty = \max \left| \frac{\tilde{w}_l - w_l}{w_l} \right|$, where $\tilde{w}_l$ and w_l represent the numerical and analytical solutions at the grid points X_l, respectively. $E_1 = |\bar{I}_1 - I_1|/|I_1|$ indicates the relative error in I_1, where $\bar{I}_1$ stands for the counterpart of I_1 by the numerical solution. The trapezoidal rule on the non-uniform mesh is employed for the evaluation of the integrals.

Example 2 (*Two Peakon Interaction*)**.** For $c = 1000$, we initially choose two approximate peakon solutions moving with velocity $v_1/2 = 2.0$, and $v_2/2 = 1.0$, respectively. Their interaction is numerically solved by MFE and RK4, respectively, with a fixed grid number of $N = 101$. Fig. 5 displays the process of collision at different times. Table 2 presents the errors in L_∞-norm and E_1. It could be seen that, in spite of a small number of grid points and a large time step, RK4 simulates the collision of two approximate peakons with good accuracy.

In regard to the propagation and interaction of approximate peakon solutions, we summarize as follows:

1. Due to the integrability of the scheme and the self-adaptive feature of the non-uniform mesh, the L_∞-norm is small and the first conserved quantity is preserved extremely well even for a small number of grid points.
2. The errors are mainly due to the time advancing methods. The MFE is first order in time, so it produces relatively large L_∞ and E_1, roughly changing in proportion with time. RK4 is fourth-order in time, so up to $T = 4.0$, L_∞ and E_1 are of the orders 10^{-12} and 10^{-13} for a grid number of $N = 101$ and a time step $\Delta t = 0.01$.

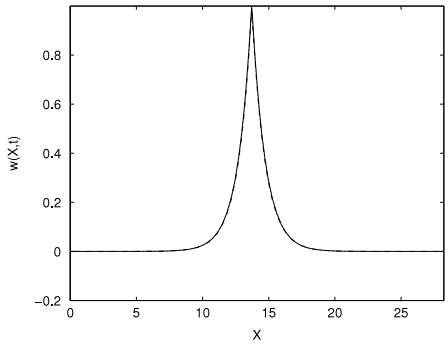

Fig. 3. Comparison between one peakon solution and one-soliton solution with $c = 200.0$.

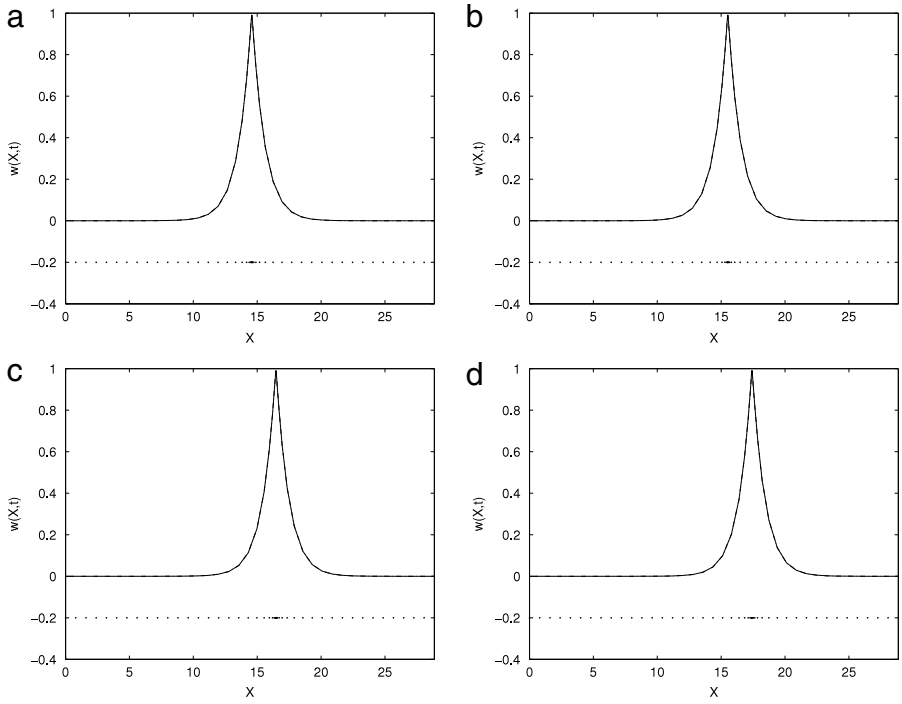

Fig. 4. Numerical solution of one single peakon solution: (a) $t = 1.0$; (b) $t = 2.0$; (c) $t = 3.0$; (d) $t = 4.0$.

4.2. Propagation and interaction of cuspon solutions

The classical 4th-order Runge–Kutta method fails whenever the cuspon solution is involved. It seems that a kind of instability occurs in this case, whose theoretical reason is still unclear. Therefore, only MFE is employed to conduct the numerical experiments hereafter.

Example 3 (*One-cuspon Propagation*)**.** The parameters taken for the one-cuspon solution are $p = 10.98, c = 10.0$. The number of grid points is taken as 101 in an interval of width of 4 in the x-domain. Through the hodograph transformation, this corresponds to an interval of width 74.34 in the X-domain. Fig. 6(a) shows the initial profile and the initial mesh. Fig. 6(b)–(d) display the numerical solutions (solid line) and exact solutions (dotted line) at $T = 2, 3, 4$, together with the self-adjusted mesh. It can be seen that the non-uniform mesh is dense around the cuspon point, and moves to the left in accordance with the movement of the cuspon point. Table 3 exhibits the results of relative errors in L_∞-norm and E_1.

Example 4 (*Two-cuspon Interaction*)**.** The parameters taken for the two-cuspon solutions are $p_1 = 11.0, p_2 = 10.5, c = 10.0$. Fig. 7(a)–(d) display the process of collision at several different times, along with the exact solution. Meanwhile, the self-adaptive mesh is also shown in the graph. It can be seen that two cuspon solutions undertake an elastic collision, regaining their shapes after the collision is complete. As mentioned in [18], the two cuspon points are always present during the collision. The grid points are automatically adapted with the movement of the cuspons, and are always concentrated

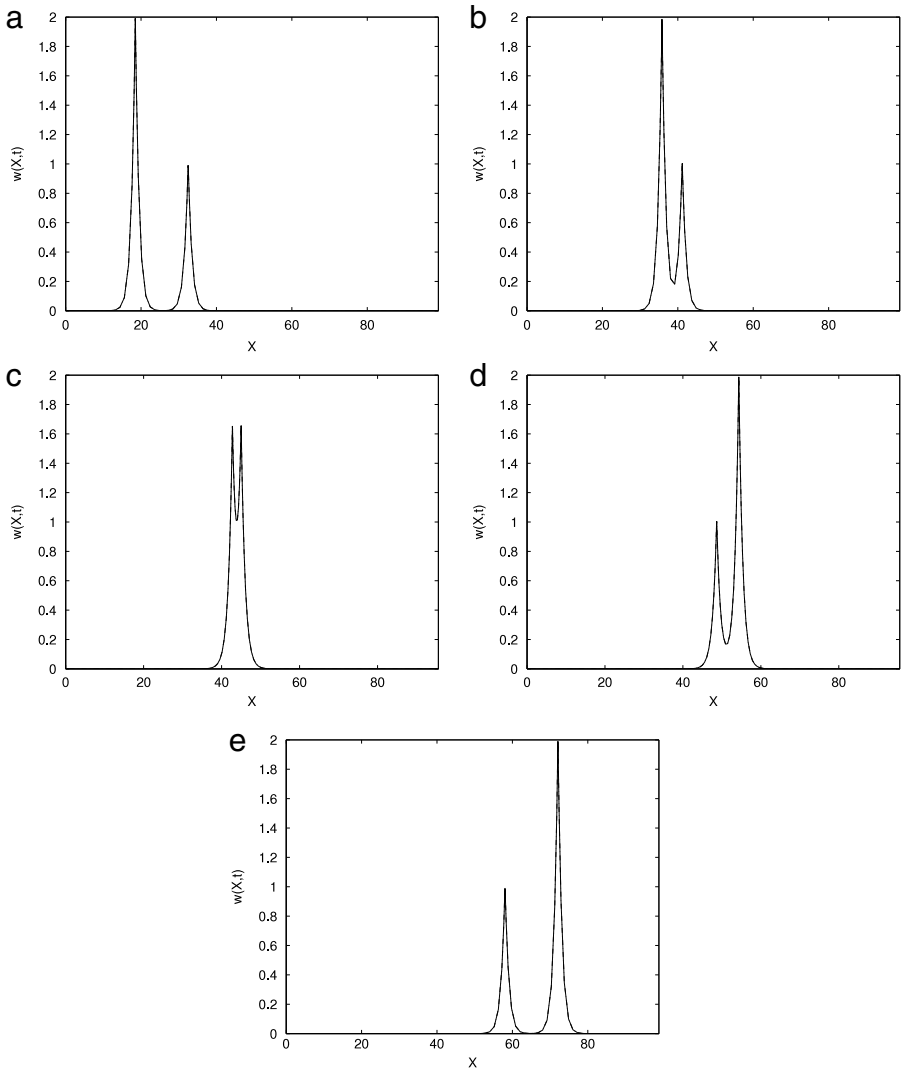

Fig. 5. Numerical solution for the collision of two nearly-peakons with $p_1 = 198.9975$, $p_2 = 199.4995$ and $c = 200.0$: (a) $t = 0.0$; (b) $t = 10.0$; (c) $t = 15.0$; (d) $t = 20.0$; (e) $t = 30.0$.

Table 3
Relative errors in L_∞ norm and the first conservative quantity for one-cuspon propagation.

Δt	T	L_∞	E_1
0.005	2.0	3.3(−2)	4.7(−2)
0.005	4.0	9.7(−2)	1.2(−1)
0.001	2.0	1.1(−2)	1.2(−2)
0.001	4.0	2.9(−2)	3.7(−2)

at the cuspon points. In compared with the exact solutions, we can comment that the numerical solutions are in a good agreement with exact solutions. As far as we know, what is shown here is the first numerical demonstration for the cuspon–cuspon interaction.

4.3. Soliton–cuspon interactions

Here we show two examples for the soliton–cuspon interaction with $c = 10.0$. In Fig. 8, we plot the interaction process between a soliton of $p_1 = 9.12$ and a cuspon of $p_2 = 10.98$ at several different times where the soliton and the cuspon have almost the same amplitude. It can be seen that when the collision starts ($t = 12.0$), another singularity point with infinite

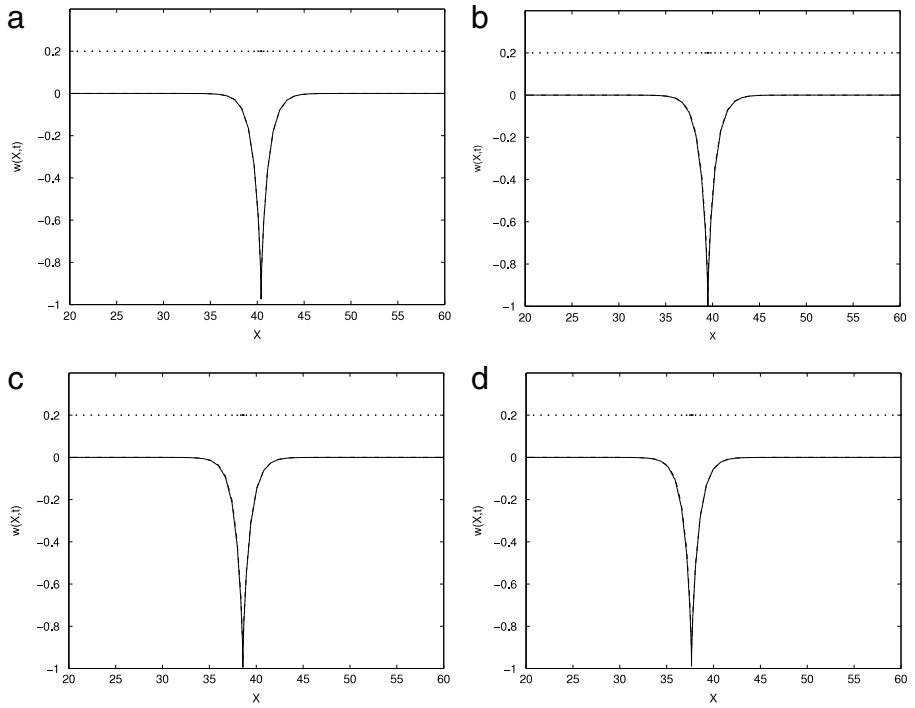

Fig. 6. Numerical and exact solutions of one single cuspon solution (solid: numerical, dotted: exact): (a) $t = 0.0$; (b) $t = 2.0$; (c) $t = 3.0$; (c) $t = 4.0$.

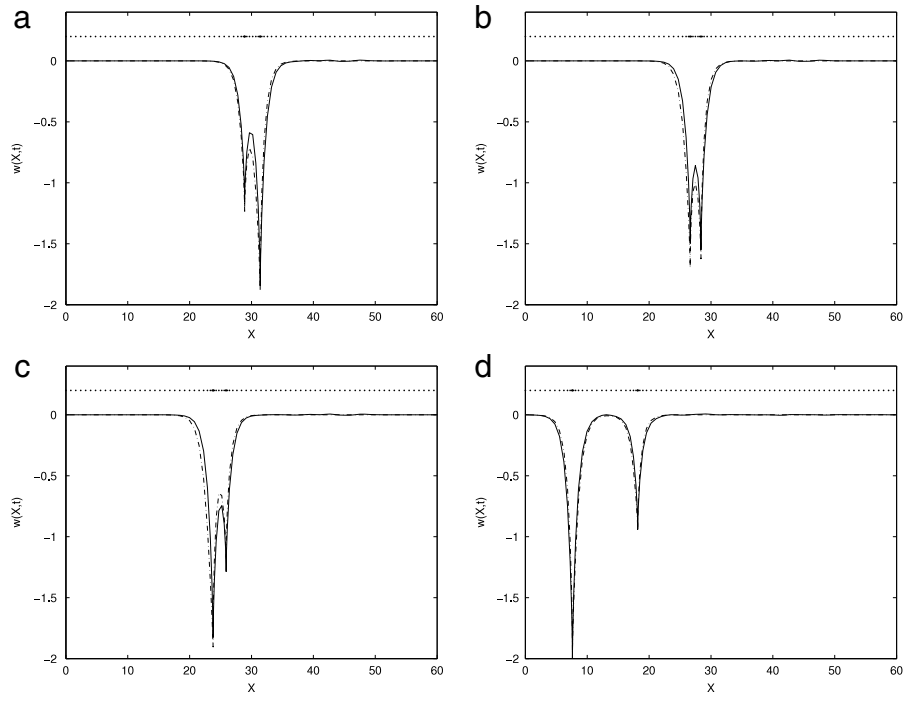

Fig. 7. Numerical and exact solutions of the collision of two-cuspon solution with $p_1 = 11.0$, $p_2 = 10.5$, $c = 10.0$ (solid: numerical, dotted: exact): (a) $t = 13.0$; (b) $t = 14.8$; (c) $t = 16.6$; (d) $t = 25.0$.

derivative (w_x) occurs. As collision goes on ($t = 14.4, 14.6, 14.8$), the soliton seems 'eats up' the cuspon, and the profile looks like a complete elevation. However, the cuspon point exists at all times, especially, at $t = 14.6$, the profile becomes one symmetrical hump with a cuspon point in the middle of the hump.

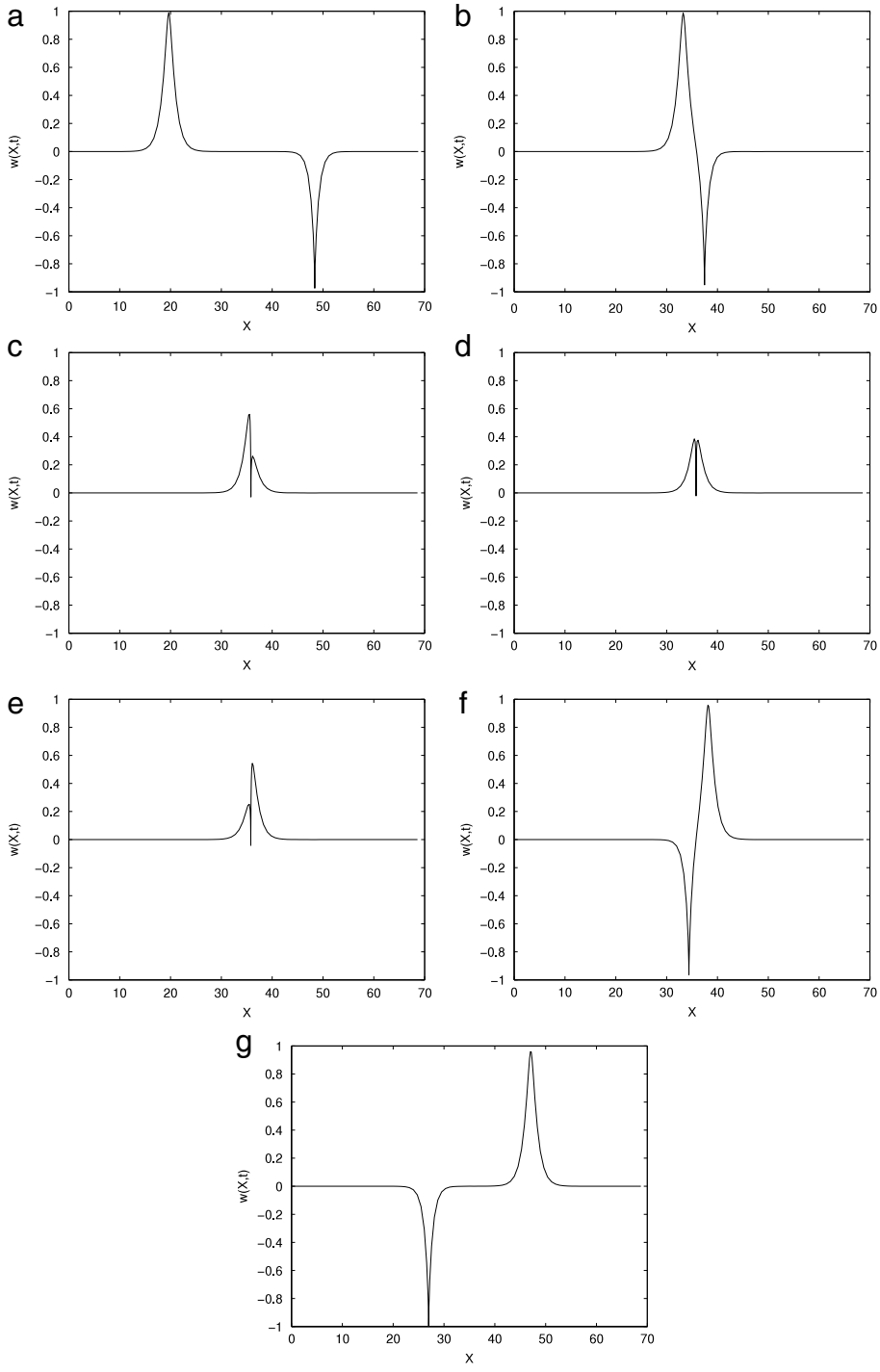

Fig. 8. Numerical solution for cuspon–soliton collision with $p_1 = 9.12$, $p_2 = 10.98$ and $c = 10.0$: (a) $t = 0.0$; (b) $t = 12.0$; (c) $t = 14.4$; (d) $t = 14.6$; (e) $t = 14.8$; (f) $t = 17.0$; (g) $t = 25.0$.

In Fig. 9, we present another example of a collision between a soliton ($p_1 = 9.12$) and a cuspon ($p_2 = 10.5$) where the cuspon has a larger amplitude (2.0) than the soliton (1.0). Again, when the collision starts, another singularity point appears. As collision goes on, the soliton is gradually absorbed by the cuspon. At $t = 10.3$, the whole profile looks like a single cuspon when the soliton is completely absorbed. Later on, the soliton reappears from the right until $t = 16$, the soliton and cuspon recover their original shapes except for a phase shift when the collision is complete.

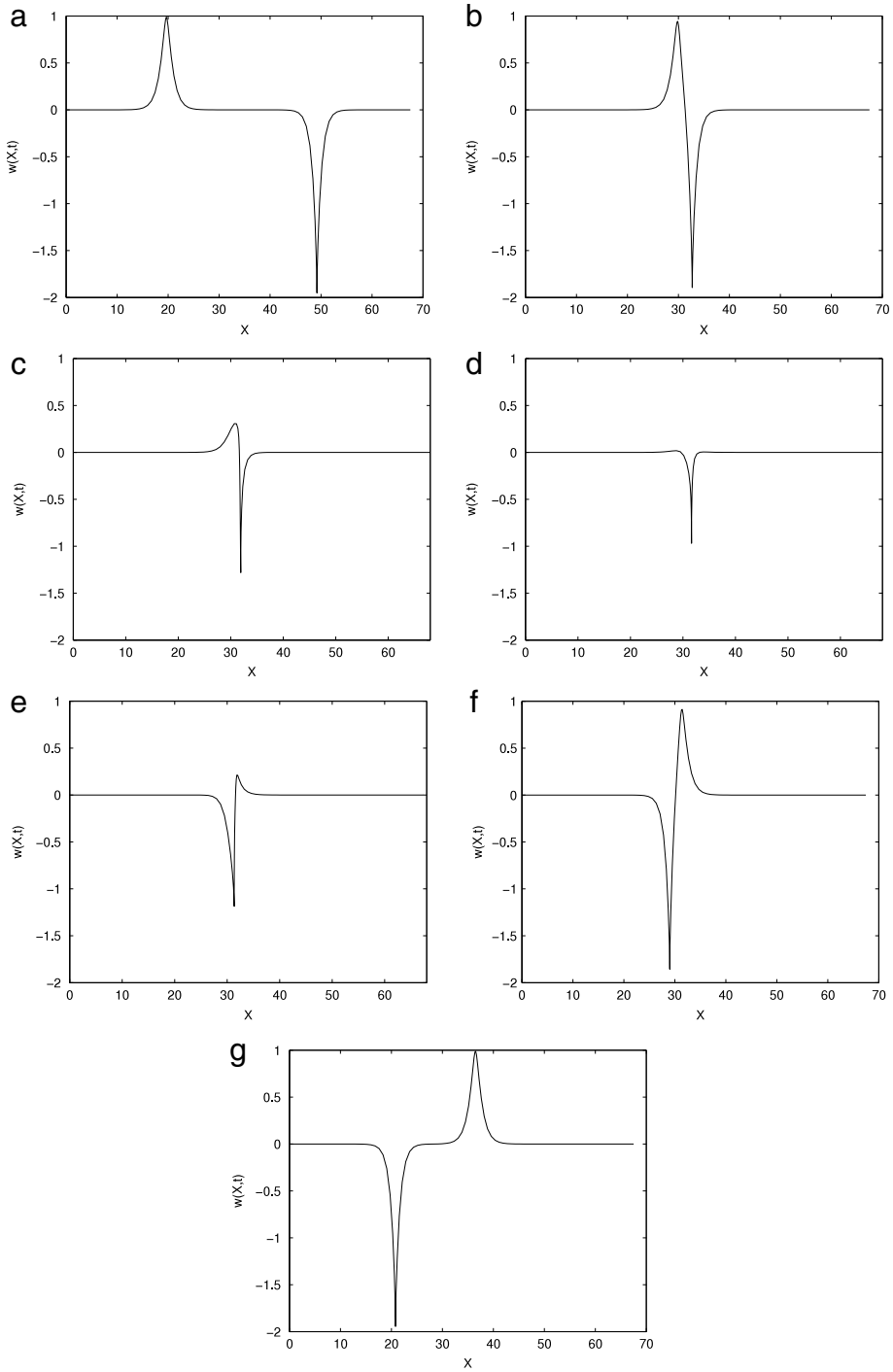

Fig. 9. Numerical solution for cuspon–soliton collision with $p_1 = 9.12$, $p_2 = 10.5$ and $c = 10.0$: (a) $t = 0.0$; (b) $t = 9.0$; (c) $t = 10.0$; (d) $t = 10.3$; (e) $t = 10.6$; (f) $t = 11.5$; (g) $t = 16.0$.

4.4. Non-exact initial value problems

Here, we show that the integrable scheme can also be applied for the initial value problem starting with non exact solutions. To the end, we choose an initial condition whose mesh size is determined by

$$\delta_k = 2ch(1 - 0.8\,\mathrm{sech}(2kh - W_x/2)), \tag{22}$$

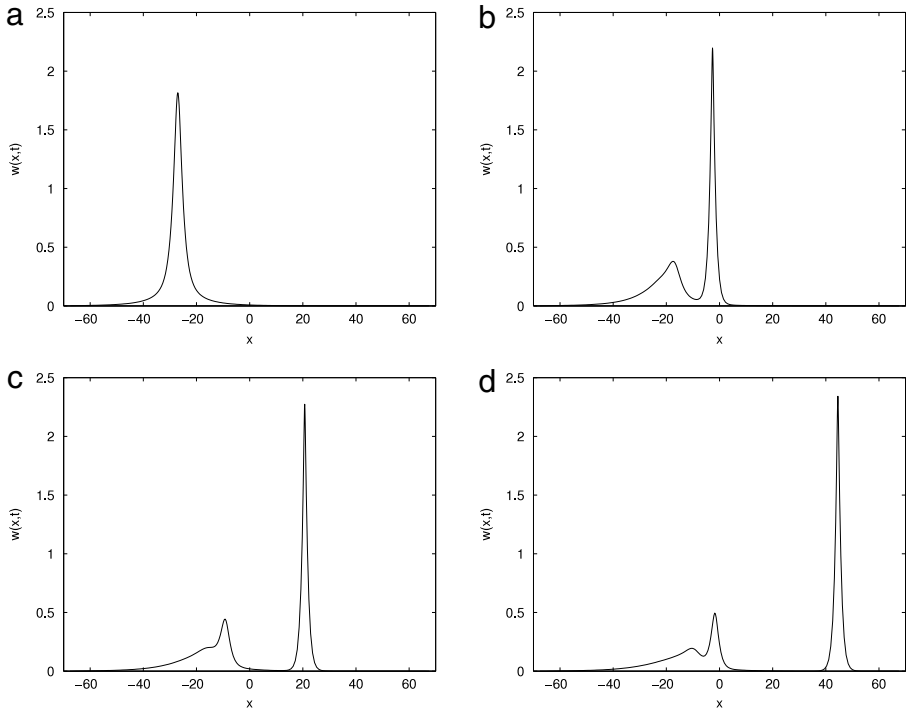

Fig. 10. Numerical solution starting from an initial condition (19) with $c = 10$: (a) $t = 0.0$; (b) $t = 10.0$; (c) $t = 20.0$; (d) $t = 30.0$.

then, the initial profile can be calculated through the second equation of the semi-discretization, which is plotted in Fig. 10 (a) Fig. 10 (b), (c) and (d) show the evolutions at $t = 10, 20, 30$, respectively. Note that $c = 10$ in this computation. It can be seen that a soliton with large amplitude is first developed, and moving fast to the right. By $t = 30$, a second soliton with small amplitude is to be developed.

Next, we increase the value of c to 90, which implies a very small dispersion term, corresponding to the dispersionless CH equation. The initial profile and the evolutions at $t = 50, 150, 200$ are shown in Fig. 11. It is seen that four nearly-peakons are developed from the initial profile at $t = 50$. Later on, an array of nearly-peakons of seven and eight are developed at $t = 150, 200$, respectively. This result is similar to the result for the KdV type equations with a small dispersion, i.e. the peakon trains are generated. (For the KdV type equations, soliton trains are generated. For example, see [44,45] for numerical simulations and [46] for a theoretical analysis for the KdV equation.) A theoretical analysis for the dispersionless CH equation to explain the above intriguing numerical result is called for.

5. Concluding remarks

In the present paper, we have proposed a self-adaptive moving mesh method for the CH equation, which based on an integrable semi-discretization of the CH equation. It has the properties: (1) it is integrable in the sense that the scheme itself admits the N-soliton solution approaching the N-soliton solution of the CH equation in the limit of mesh size going to zero; (2) the mesh is non-uniform and is automatically adjusted so that it is concentrated in the region where the solution changes sharply, for example, the cuspon point; (3) once the non-uniform mesh is evolved, the solution is determined from the evolved mesh by solving a tridiagonal linear system. Therefore, either from the accuracy or from the computation cost, the proposed method is expected to be superior than other existing numerical methods of the CH equation. This is indeed true. The numerical results in this paper indicate that a very good accuracy is obtained.

Two time advancing methods, the modified forward Euler method and the classical 4th-order Runge–Kutta method, are used to solve the evolution of non-uniform mesh. The Runge–Kutta method gains much better accuracy than the modified forward Euler method. However, it fails for the computations of cuspons. Using the self-adaptive moving mesh method for the CH equation, we have obtained interesting numerical computation results starting with non-exact solutions. When κ is very small, the peakon train is generated from the non-exact initial condition.

As further topics, it is interesting to construct integrable discretizations, or, the self-adaptive moving mesh methods for a class of integrable nonlinear wave equations possessing soliton solutions with singularities such as peakon, cuspon or loop solutions. For example, such equations include the short pulse equation which was derived as a model for the propagation

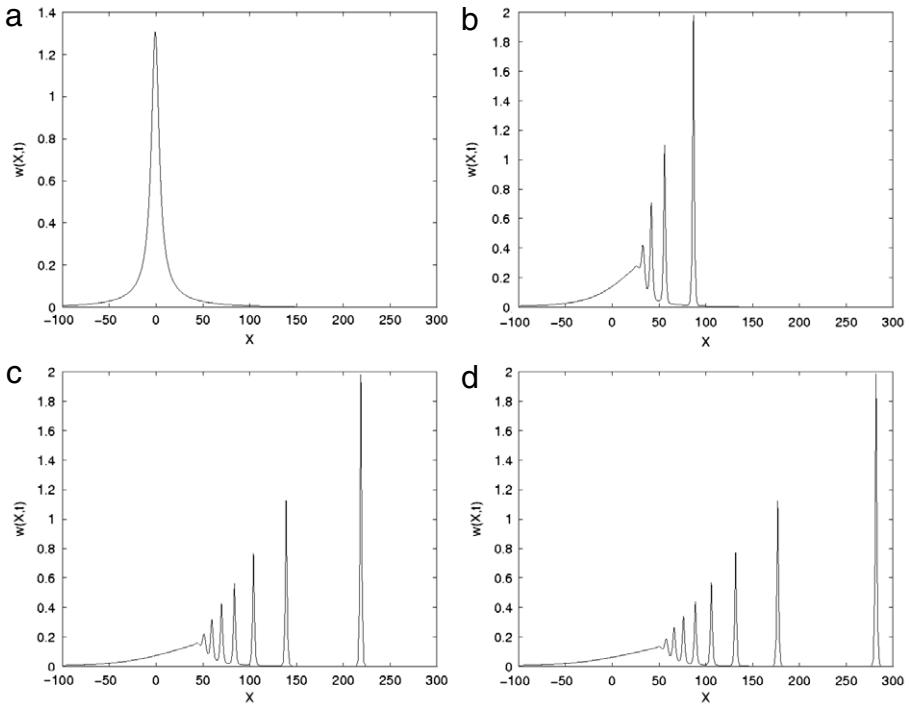

Fig. 11. Numerical solution starting from an initial condition (19) with $c = 90$: (a) $t = 0.0$; (b) $t = 50.0$; (c) $t = 150.0$; (d) $t = 200.0$.

of ultra-short optical pulses in nonlinear media [47],

$$u_{XT} = u + \frac{1}{6}(u^3)_{XX}, \tag{23}$$

and the Degasperis–Procesi (DP) equation [48]

$$u_T + 3\kappa^3 u_X - u_{TXX} + 4uu_X = 3u_X u_{XX} + uu_{XXX}. \tag{24}$$

It is worth pointing out that the authors have constructed semi- and full-discretization for the short pulse equation, which is another example of the self-adaptive moving mesh method [49], in which we have succeeded in computing the one- and two-loop soliton propagations and interactions.

Acknowledgements

The work of B.F. was partially supported by the US Army Research Office under Contract No. W911NF-05-1-0029. The work of Y.O. was partly supported by JSPS Grant-in-Aid for Scientific Research (B-19340031, S-19104002). Y.O. and K.M. are grateful for the hospitality of the Isaac Newton Institute for Mathematical Sciences (INI) in Cambridge where this article was completed during the programme Discrete Integrable Systems (DIS). The authors are grateful to the anonymous referee for valuable comments.

References

[1] R. Camassa, D.D. Holm, An integrable shallow water equation with peaked solitons, Phys. Rev. Lett. 71 (1993) 1661–1664.
[2] B. Fuchssteiner, A. Fokas, Symplectic structures, their Bäcklund transformations and hereditary symmetries, Physica D 4 (1981) 47–66.
[3] R.S. Johnson, Camassa–Holm, Korteweg–deVries and related models for waterwaves, J. Fluid Mech. 457 (2002) 63–82.
[4] A. Constantin, D. Lannes, The hydrodynamical relevance of the Camassa–Holm and Degasperis–Procesi equations, Arch. Ration. Mech. Anal. 192 (2009) 165–186.
[5] R.S. Johnson, The Camassa–Holm equation for water waves moving over a shear flow, Fluid Dynam. Res. 33 (2003) 97–111.
[6] V. Busuioc, On second grade fluids with vanishing viscosity, C. R. Acad. Sci. Paris Ser. I 328 (1999) 1241–1246.
[7] H.-H. Dai, Exact travelling-wave solutions of an integrable equation arising in hyperelastic rods, Wave Motion 28 (1998) 367–381.
[8] A. Constantin, On the scattering problem for the Camassa–Holm equation, Proc. R. Soc. Lond. Ser. A 457 (2001) 953–970.
[9] A. Constantin, V.S. Gerdjikov, R.I. Ivanov, Inverse scattering transform for the Camassa–Holm equation, Inverse Problems 22 (2006) 2197–2207.
[10] R. Camassa, D.D. Holm, J.M. Hyman, A new integrable shallow water equation, Adv. Appl. Mech. 31 (1994) 1–33.
[11] R. Beals, D.H. Sattinger, J. Szmigielski, Multipeakons and the classical momemt problem, Adv. Math. 154 (2000) 229–257.
[12] J. Schiff, The Camassa–Holm equation: a loop group approach, Physica D 121 (1998) 24–43.
[13] M.C. Ferreira, R.A. Kraenkel, A.I. Zenchuk, Soliton–cuspon interaction for the Camassa–Holm equation, J. Phys. A: Math. Gen. 32 (1999) 8665–8670.
[14] R.S. Johnson, On solutions of the Camassa–Holm equation, Proc. R. Soc. Lond. Ser. A 459 (2003) 1687–1708.

[15] Y. Li, J.E. Zhang, The multiple-soliton solution of the Camassa–Holm equation, Proc. R. Soc. Lond. Ser. A 460 (2004) 2617–2627.
[16] A. Parker, On the Camassa–Holm equation and a direct method of solution. I. Bilinear form and solitary waves, Proc. R. Soc. Lond. Ser. A 460 (2004) 2929–2957.
[17] A. Parker, On the Camassa–Holm equation and a direct method of solution. II. Soliton solutions, Proc. R. Soc. Lond. Ser. A 461 (2005) 3611–3632.
[18] H.-H. Dai, Y. Li, The interaction of the ω-soliton and the ω-cuspon of the Camassa–Holm equation, J. Phys. A: Math. Gen. 38 (2005) L685–L694.
[19] Y. Matsuno, Parametric representation for the multisoliton solution of the Camassa–Holm equation, J. Phys. Soc. Japan 74 (2005) 1983–1987.
[20] H. Kalisch, J. Lenells, Numerical study of traveling-wave solutions for the Camassa–Holm equation, Chaos Solitons Fractals 25 (2005) 287–298.
[21] H. Holden, X. Raynaud, Convergence of a finite difference scheme for the Camassa–Holm equation, SIAM J. Numer. Anal. 44 (2006) 1655–1680.
[22] G.M. Coclite, K.H. Karlsen, N.H. Risebro, A convergent finite difference scheme for the Camassa–Holm equation with general H^1 initial data, SIAM J. Numer. Anal. 46 (2008) 1554–1579.
[23] R. Artebrant, H.J. Schroll, Numerical simulation of Camassa–Holm peakons by adaptive upwinding, Appl. Numer. Math. 56 (2006) 695–711.
[24] Y. Xu, C.-W. Shu, A local discontinuous Galerkin method for the Camassa–Holm equation, SIAM J. Numer. Anal. 46 (2008) 1998–2021.
[25] T. Matsuo, H. Yamaguchi, An energy-conserving Galerkin scheme for a class of nonlinear dispersive equations, J. Comput. Phys. 228 (2009) 4336–4358.
[26] T. Matsuo, A Hamiltonian-conserving Galerkin scheme for the Camassa–Holm, J. Comput. Appl. Math. 234 (2009) 1258–1266.
[27] D. Cohen, B. Owren, X. Raynaud, Multi-symplectic integration of the Camassa–Holm equation, J. Comput. Phys. 227 (2008) 5492–5512.
[28] R. Camassa, Characteristics and the initial value problem of a completely integrable shallow water equation, Discrete Contin. Dyn. Syst. Ser. B 3 (2003) 115–139.
[29] R. Camassa, J. Huang, L. Lee, On a completely integrable numerical scheme for a nonlinear shallow-water wave equation, J. Nonlinear Math. Phys. 12 (2005) 146–162.
[30] R. Camassa, J. Huang, L. Lee, Integral and integrable algorithms for a nonlinear shallow-water wave equation, J. Comput. Phys. 216 (2006) 547–572.
[31] R. Camassa, L. Lee, Complete integrable particle methods and the recurrence of initial states for a nonlinear shallow-water wave equation, J. Comput. Phys. 227 (2008) 7206–7221.
[32] H. Holden, X. Raynaud, A convergent numerical scheme for the Camassa–Holm equation based on multipeakons, Discrete Contin. Dyn. Syst. 14 (2006) 505–523.
[33] Y. Ohta, K. Maruno, B.-F. Feng, An integrable semi-discretization of the Camassa–Holm equation and its determinant solution, J. Phys. A 41 (2008) 355205.
[34] A. Harten, J.M. Hyman, Self-adjusting grid methods for one-dimensional hyperbolic conservation laws, J. Comput. Phys. 50 (1983) 235–315.
[35] K. Miller, R.N. Miller, Moving finite elements. I, SIAM J. Numer. Anal. 18 (1981) 1019–1032.
[36] E.A. Dorfi, T.J. Kaper, Simple adaptive grids for 1-D initial value problems, J. Comput. Phys. 69 (1987) 175–195.
[37] J.U. Brackbill, An adaptive grid with directional control, J. Comput. Phys. 108 (1993) 38–50.
[38] W.M. Cao, W.Z. Huang, R.D. Russell, An r-adaptive finite element method based upon moving mesh PDEs, J. Comput. Phys. 149 (1999) 221–244.
[39] J.M. Stockie, J.A. Mackenzie, R.D. Russell, A moving mesh method for one dimensional hyperbolic conservation laws, SIAM J. Sci. Comput. 22 (2001) 1791–1813.
[40] H.Z. Tang, T. Tang, Adaptive mesh methods for one- and two-dimensional hyperbolic conservation laws, SIAM J. Numer. Anal. 41 (2003) 487–515.
[41] Y. Matsuno, The peakon limit of the N-soliton solution of the Camassa–Holm equation, J. Phys. Soc. Japan 76 (2007) 034003.
[42] Y. Li, P. Olver, Convergence of solitary wave solutions in a perturbed bi-Hamiltonian dynamical system. I. Compactons and peakons, Discrete Contin. Dyn. Syst. Ser. A 3 (1997) 419–432.
[43] A. Parker, Y. Matsuno, The peakon limits of soliton solutions of the Camassa–Holm equation, J. Phys. Soc. Japan 75 (2006) 124001.
[44] A.M. Kamchatnov, R.A. Kraenkel, B.A. Umarov, Asymptotic soliton train solution of Kaup–Boussinesq equations, Wave Motion 38 (2003) 355–365.
[45] G.A. El, R.H.J. Grimshaw, N.F. Smyth, Asymptotic description of solitary wave trains in fully nonlinear shallow-water theory, Physica D 237 (2008) 2423–2435.
[46] V.I. Karpman, An asymptotic solution of the Korteweg–de Vries equation, Phys. Lett. A 25 (1967) 708–709.
[47] T. Schäfer, C.E. Wayne, Propagation of ultra-short optical pulses in cubic nonlinear media, Physica D 196 (2004) 90–105.
[48] A. Degasperis, M. Procesi, Asymptotic integrability, in: A. Degasperis, G. Gaeta (Eds.), Symmetry and Perturbation Theory, World Scientific, Singapore, 1999, pp. 23–37.
[49] B.-F. Feng, K. Maruno, Y. Ohta, Integrable discretizations of the short pulse equation, J. Phys. A 43 (2010) 085203.